

JGR Atmospheres

RESEARCH ARTICLE

10.1029/2021JD035538

Key Points:

- Both traveling and stationary planetary waves with zonal wavenumber 1 seem to play a salient role in preconditioning the warming event
- Existing instability is believed to support the growth of the quasi-6-day wave (Q6DW) in post warming interval
- The Q6DW and Q16DW are found to propagate from high and mid latitudes to low latitudes during the warming

Correspondence to:

G. Mitra,
reachmitragourav@gmail.com

Citation:

Mitra, G., Guharay, A., Batista, P. P., & Buriti, R. A. (2022). Impact of the September 2019 minor sudden stratospheric warming on the low-latitude middle atmospheric planetary wave dynamics. *Journal of Geophysical Research: Atmospheres*, 127, e2021JD035538. <https://doi.org/10.1029/2021JD035538>

Received 7 JUL 2021
Accepted 14 DEC 2021

Author Contributions:

Conceptualization: G. Mitra, A. Guharay
Data curation: R. A. Buriti
Formal analysis: G. Mitra
Resources: P. P. Batista
Supervision: A. Guharay
Writing – review & editing: P. P. Batista, R. A. Buriti

Impact of the September 2019 Minor Sudden Stratospheric Warming on the Low-Latitude Middle Atmospheric Planetary Wave Dynamics

G. Mitra^{1,2} , A. Guharay¹ , P. P. Batista³ , and R. A. Buriti⁴

¹Space and Atmospheric Sciences Division, Physical Research Laboratory, Ahmedabad, India, ²Department of Physics, Indian Institute of Technology, Gandhinagar, India, ³Heliophysics, Planetary Sciences and Aeronomy Division, National Institute for Space Research, INPE, São José Dos Campos, Brazil, ⁴Department of Physics, Federal University of Campina Grande, Campina Grande, Brazil

Abstract Planetary wave (PW) associated dynamical variability in the equatorial and extratropical middle atmosphere during the September 2019 Southern hemisphere minor sudden stratospheric warming (SSW) is investigated utilizing meteor radar wind observations from São João do Cariri (7.4°S, 36.5°W) and Cachoeira Paulista (22.7°S, 45°W) and reanalysis data. Signature of the mesospheric warming in conjunction with the stratospheric cooling is found at low latitudes. The strong westerly wind at low latitudes decelerates notably near 65 km at the onset of the warming episode, although no wind reversal is observed. The wind spectra reveal a prevalent quasi-16-day wave (Q16DW) prior to the SSW and existence of a quasi-6-day wave (Q6DW) after the warming event. Possible existence of barotropic/baroclinic instability in the low and mid latitude middle atmosphere may be responsible for exciting the Q6DW. Both traveling and stationary waves exhibit notable activities during the warming event. Although involvement of both zonal wavenumbers 1 and 2 PWs are found in the event, PW with zonal wavenumber 1 seems to play a vital role in preconditioning the same. Furthermore, significant latitudinal mixing of air mass between the tropics and high latitudes is evident in the potential vorticity map. The Eliassen-Palm flux diagnosis shows the propagation of the Q6DW and Q16DW from mid to low latitudes during the warming event.

Plain Language Summary A minor but impactful sudden stratospheric warming event occurred in the Southern hemisphere during September 2019. This event is characterized by a marked deceleration of the zonal mean westerlies at polar stratosphere although no wind reversal is observed. Simultaneously, stratospheric temperature at high latitudes increases sharply by more than 25 K within a few days. During the same warming event, stratospheric cooling and mesospheric warming is found at the present low latitude stations. The wind spectra reveal a long period wave of about 16 days prior to the warming event in the stratosphere followed by a relatively shorter period wave (~6 days) in the mesosphere. The 6-day wave component is possibly excited due to the instability in the middle atmosphere at low and middle latitudes during the warming episodes. Both traveling and stationary large-scale waves are supposed to play a vital role in preconditioning the warming event. There is also significant meridional air mass mixing during the warming days owing to possible planetary wave (PW) driven weakening of the zonal mean westerlies. The PW fluxes for both the aforementioned components are observed to propagate from high and mid to low latitudes during the warming event.

1. Introduction

Sudden stratospheric warming (SSW) is a dramatic episode in the winter stratosphere, which involves an abrupt increase in polar stratospheric temperature by a few tens of kelvin in several days (Andrews et al., 1987). The SSW was first reported by Scherhag (1952) using radiosonde observations. Major and minor warmings are two main categories of the SSW event. Reversal of temperature gradient poleward of 60° is a signature of both major and minor events, but the reversal of zonal mean zonal wind at 60° latitude and 10 hPa pressure level is the characteristics of a major warming (Labitzke et al., 2005). The occurrence of SSW is more frequent in the Northern hemisphere (NH) than the Southern hemisphere (SH) because of higher planetary wave (PW) activity due to topographic difference and land-sea contrast. Also, the cumulative wave flux requirement to cause SSW

in SH is supposed to be much larger because of stronger SH polar jet as compared to the NH counterpart (Rao et al., 2019).

It is well known that the abnormal change in the stratospheric temperature and the zonal wind due to anomalous PW activity during the SSW has a significant effect on the dynamical variability of the middle atmosphere (Pedatella et al., 2018). Impact of the SSW on the mesosphere and lower thermosphere (MLT) from the NH mid and high latitudes is reported by a handful of previous literatures (Whiteway & Carswell, 1994; Hoffmann et al., 2002). However, a very few studies from the SH mid and high latitudes are available to date (Dowdy et al., 2004). Fritz and Soules (1970) were the first to report the influence of the polar disturbances caused by the SSW on the tropical atmosphere. Past studies found stratospheric cooling in the tropics during the SSW event (Andrews et al., 1987; Guharay & Batista, 2019). There are quite a few investigations on the coupling between low and high latitude middle atmosphere during the SSW event in the NH (Guharay & Sekar, 2012; Kode-ra, 2006; Sivakumar et al., 2004).

Until now, in the SH, one major SSW occurred in 2002 (Dowdy et al., 2004). Furthermore, observational studies on the response of the tropical middle atmosphere during major SSW from the SH are insufficient (Guharay et al., 2014; Guharay & Batista, 2019) and hence more investigations from low latitudes are required to understand low and high latitudes coupling during such dramatic event. Recently, a minor but impactful SSW event occurred in the SH in September 2019 (Lim et al., 2020; Yamazaki et al., 2020). Interestingly, Noguchi et al. (2020) reported substantial enhancement of convective activity in the tropics of the summer hemisphere during the 2019 SH minor warming episode. The 2019 SSW event offered a suitable condition to study the ionospheric variability due to forcing from the lower and middle atmosphere owing to its occurrence during a period of low solar activity (Goncharenko et al., 2020).

Most recently, Yamazaki et al. (2020) observed a quasi-6-day wave (Q6DW) forcing from the middle atmosphere to cause ionospheric variability during the 2019 September warming event. Miyoshi and Yamazaki (2020) concluded that the non-linear interaction between the Q6DW and migrating semidiurnal tide as the excitation mechanism of the 6-day oscillation in the ionosphere during the same event. Unfortunately, the features of the dynamical variability in the middle atmosphere, especially at low latitude during the same event is not yet explored.

Therefore, in our present study, we aim to investigate the PW associated dynamical variability in the equatorial and extratropical middle atmosphere during the September 2019 minor SSW event utilizing meteor radar wind observations from São João do Cariri (7.4°S, 36.5°W) (CA) and Cachoeira Paulista (22.7°S, 45°W) (CP) and global reanalysis data set. Our present study is important in view of the lack of adequate understanding related to the impact of the SSW on the SH low latitude middle atmosphere dynamics.

2. Observational Database

For the present study, we have utilized two databases during the period centered around the minor warming episode ~ from 1 August to 31 October (2019), as described below.

2.1. Meteor Radar

The radar systems at CA and CP are all-sky interferometric meteor radars which operate at a frequency of 35.24 MHz, with pulse width of 13 μ s, pulse repetition frequency of 2 kHz and peak power of 12 kW. It consists of a single three-element Yagi antenna for transmission and five phase-coherent two-element Yagi receiving antennas. The receiving antennas are aligned along two orthogonal baselines with the central one common to both for detecting the echo signal from the meteors. Details of the derivation of the horizontal winds from the meteor trail echoes can be found in the available literature (Hocking et al., 2001). For the present work, we have utilized horizontal wind values within the altitude range 81–99 km with a vertical resolution of 3 km and a temporal resolution of 1 hr.

2.2. ERA5 Database

The ERA5 database provides reanalysis data of various atmospheric parameters available from 1979 to the present time provided by the European Center for Medium-range Weather Forecasts (ECMWF) (Hersbach et al., 2020).

For the present investigation, we have used temperature, zonal wind and meridional wind at 137 model pressure levels within the range 1,000–0.01 hPa (~0–80 km) with a latitudinal and longitudinal grid of $0.1^\circ \times 0.1^\circ$. The closest grid points to CP and CA are chosen as (22.7°S, 45°W) and (7.4°S, 36.5°W) respectively. Thus, the analysis of ERA5 data set is aimed to complement the meteor radar observation for providing a holistic picture of the dynamical variability in the lower and middle atmosphere. Furthermore, the ERA5 global database offers the opportunity to investigate the latitudinal coupling between high and low latitude during such a dynamical event.

3. Results

To identify heating/cooling in a qualitative manner the differences between the zonal mean temperature and temporal mean (August–October 2019) of zonal mean temperature at 10 hPa pressure level in the SH, using the ERA5 data set, are plotted during the interval 1 August to 31 October 2019 (Day of year [DOY] 213 = 1 August) in Figure 1a. At high latitude ($>75^\circ\text{S}$), the temperature difference is mostly negative from DOY 213 to DOY 248. It becomes positive with the maximum warming on 18 September (DOY 261), and the warming persists for the remaining period of study. Noticeable warming greater than 25 K exists between DOY 253 and DOY 263, which is considered as the warming period (SSW event) in our present study as per the criteria defined by McInturff (1978), that is, a temperature increase of at least 25 K in a week or less at any stratospheric altitudes in any region of winter hemisphere. Such warming at mid and high latitudes corresponds to cooling during the period between DOY 243 and DOY 263 in the tropical area, which is the topic of interest in this paper. Relative cooling between DOY 243 and DOY 263 at 10 hPa at low latitudes ($<30^\circ\text{S}$) can be noted from Figure 1a. Figure 1b shows the zonal mean zonal wind during the above-mentioned period at 10 hPa. The strong eastward wind at 10 hPa, 60°S decelerates monotonously by 70 m s^{-1} (approx.) till the end of warming, that is, DOY 263, although there is no wind reversal. The altitudinal profiles of difference between zonal mean temperature and temporal mean of zonal mean temperature at 60°S, 22.7°S (CP latitude) and 7.4°S (CA latitude) are shown in Figures 1c, 1e and 1g, respectively. Similarly, the altitudinal profiles of the zonal mean zonal wind at 60°S, 22.7°S (CP latitude) and 7.4°S (CA latitude) are shown in Figures 1d, 1f, and 1h, respectively. Following observations are noteworthy.

1. At 60°S (Figure 1c), remarkable increase of temperature can be noted in the mid-stratosphere (20–40 km) during the warming period that continues for the remaining period of observations, whereas there is significant cooling at mesospheric altitudes concurrent with the stratospheric warming
2. Westerly wind at 60°S (Figure 1d) diminishes in magnitude at the advent of the warming event in the middle atmosphere with a reversal in the zonal wind at altitudes in the upper stratosphere as prominent during the SSW event. Therefore, the present minor warming episode can be termed high stratospheric warming (Savenkova et al., 2017)
3. However, the low latitude middle atmosphere (Figures 1e and 1g) shows contrasting behavior with respect to high latitude, that is, cooling in the stratosphere coincident with the high latitude warming and warming in the mesosphere concurrent with the high latitude cooling
4. The zonal wind at low latitude (Figures 1f and 1h), especially, at CP near 50–70 km altitude shows noticeable weakening with the advent of the warming. However, at lower latitude (CA) such effect is very weak and exists over narrow altitude region near 65 km

To determine the involvement of traveling PWs (if any) over the present locations, a wavelet analysis using Morlet as a mother wavelet is carried out for the observational interval. Figures 2a–2c and 2d show the wavelet power spectra for zonal wind at 90 km, 0.02 hPa (~80 km), 1 hPa (~48 km) and 10 hPa (~32 km), respectively at CP. Bold white curves in each plot represent 95% confidence level. It is clear from Figure 2a that a Q6DW (also observed by Yamazaki et al. (2020) in the ionosphere) with periods 5–7 days becomes prominent in mid-MLT (90 km) just after the warming, that exists for a few days. At 0.02 hPa (near mesopause), zonal wind wavelet spectrum at CP shows a strong quasi-10-day wave (Q10DW) with periods 9–12 days before the warming event and a relatively weaker Q6DW which exists during and after the warming event as seen in Figure 2b. A quasi-16-day wave (Q16DW) with periodicity in the range 14–20 days exists in the prewarming condition in the mesopause region (0.02 hPa) with lesser strength. Wavelet power spectra for the zonal wind exhibits the Q16DW at 1 hPa (upper stratosphere) before the warming event and weakens in the following interval (Figure 2c). Almost similar feature is observed at 10 hPa, as seen in Figure 2d. The strength of the Q16DW is greater at 1 hPa than that at 10 hPa. Figures 2e–2g and 2h show the meridional wind wavelet spectra at CP at 90 km, 0.02 hPa, 1 hPa and

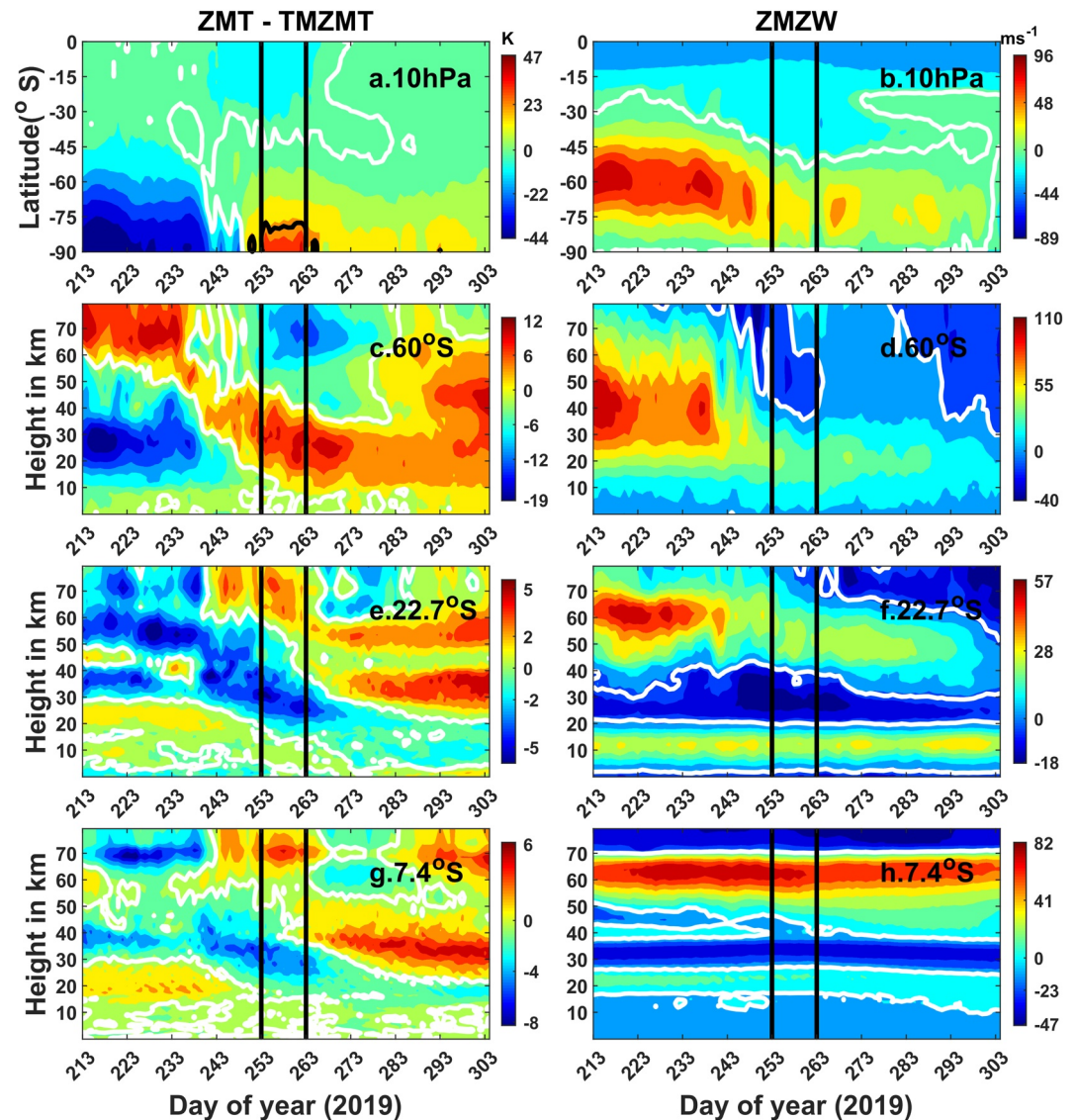


Figure 1. (a) Difference between the zonal mean temperature and temporal mean of zonal mean temperature (ZMT–TMZMT) during August–October 2019 (DOY 213–1 August) and (b) zonal mean zonal wind (ZMWZ) plotted during the same period at 10 hPa pressure level using ERA5. Altitudinal profiles (~0–80 km) of difference between the zonal mean temperature and temporal mean of zonal mean temperature are shown at (c) 60°S, (e) 22.7°S (CP latitude) and (g) 7.4°S (CA latitude). Similarly, altitudinal profiles (~0–80 km) of zonal mean zonal wind are shown at (d) 60°S, (f) 22.7°S (CP latitude) and (h) 7.4°S (CA latitude). The white bold curves represent zero value in all the plots, and the bold black curve represents a value of 25 K in Figure 1a. Region between two vertical lines shows warming period for the present and all the following figures. Please note the change of scale in the colorbars corresponding to each subplot while comparing.

10 hPa, respectively. The Q6DW is observed to be well distributed around the warming days in the mid-MLT region, as seen in Figure 2e. At 0.02 hPa pressure level near the mesopause (Figure 2f), there is a Q10DW during the pre-warming interval, followed by the appearance of a Q6DW which intensifies at the end of warming and continues till DOY 273. In the upper stratosphere at 1 hPa pressure level (Figure 2g), the meridional wind wavelet spectrum exhibits a strong Q16DW before the warming episodes, which weakens by the end of the warming. At 10 hPa (Figure 2h), the Q6DW is found to be dominant for a few days during the pre-warming time and again reappears with comparatively lesser intensity during the warming days, and, the Q16DW appears during the warming days. Additionally, there exists a weak quasi-3-day wave (Q3DW) with periodicity of 3–4 days after the warming event for a short while. Overall, the zonal wind wavelet spectra show robust wave activity in terms of power as compared to the meridional wind wavelet spectra.

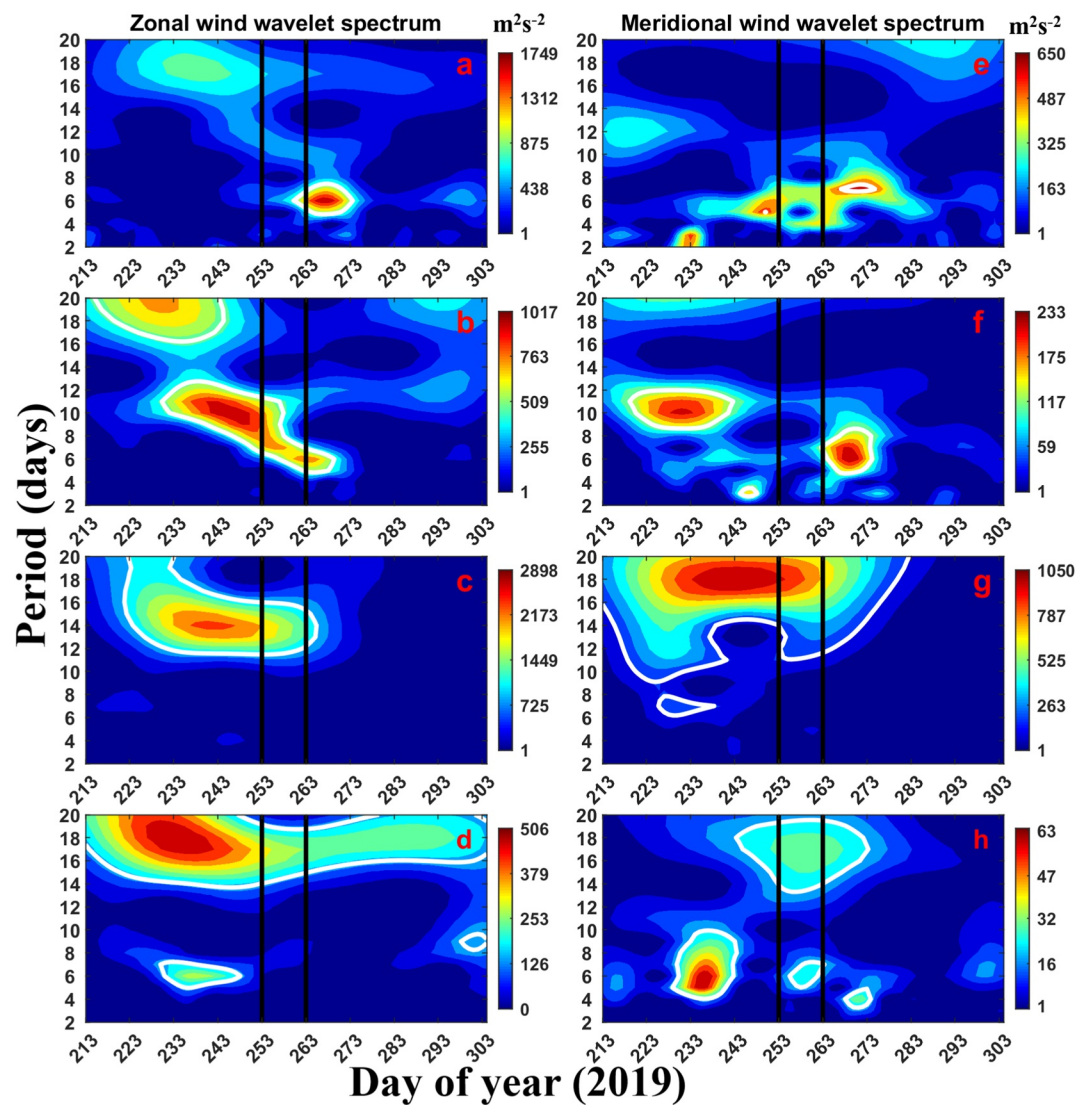


Figure 2. Wavelet power spectra at 90 km for (a) zonal wind, (e) meridional wind using meteor radar. Wavelet spectra in the zonal wind at (b) 0.02 hPa, (c) 1 hPa, (d) 10 hPa and meridional wind at (f) 0.02 hPa, (g) 1 hPa, (h) 10 hPa at CP using ERA5. Bold white curves in each plot represent 95% confidence level. Please note the change of scale in the colorbars corresponding to each subplot while comparing.

Similarly, Figures 3a–3c and 3d represent the zonal wind wavelet spectra for CA at 90 km, 0.02 hPa, 1 hPa and 10 hPa, respectively. The Q10DW feature is significant at 90 km (Figure 3a) during warming days, but its magnitude is lesser as compared to the Q6DW which is present during a short interval following the warming. Enhancement of the Q6DW in the zonal wind wavelet spectrum in the mesopause (0.02 hPa) during a short interval after the warming days is evident from Figure 3b. The Q16DW activity is dominant in the upper stratosphere (1 hPa) before warming days and vanishes at the onset of the warming event (Figure 3c). In the mid-stratosphere (10 hPa) the Q10DW is present throughout the observational period except an interval of around 10 days before the warming onset. On the other hand, the Q16DW enhances during warming days and weakens after the warming, as seen in Figure 3d. Figures 3e–3g and 3h illustrate the PW features in the meridional wind over CA at 90 km, 0.02, 1 and 10 hPa, respectively. There are weak traces of the Q6DW around the warming days at 90 km (Figure 3e). The Q3DW is present before the onset of warming at 0.02 hPa pressure level (Figure 3f). In the upper stratosphere at 1 hPa, the Q16DW is present before the warming days. At the same altitude, the Q3DW becomes significant between DOY 233 and DOY 243, as shown in Figure 3g. The Q3DW is found to be significant before, during and after the warming event at 10 hPa pressure level (Figure 3h).

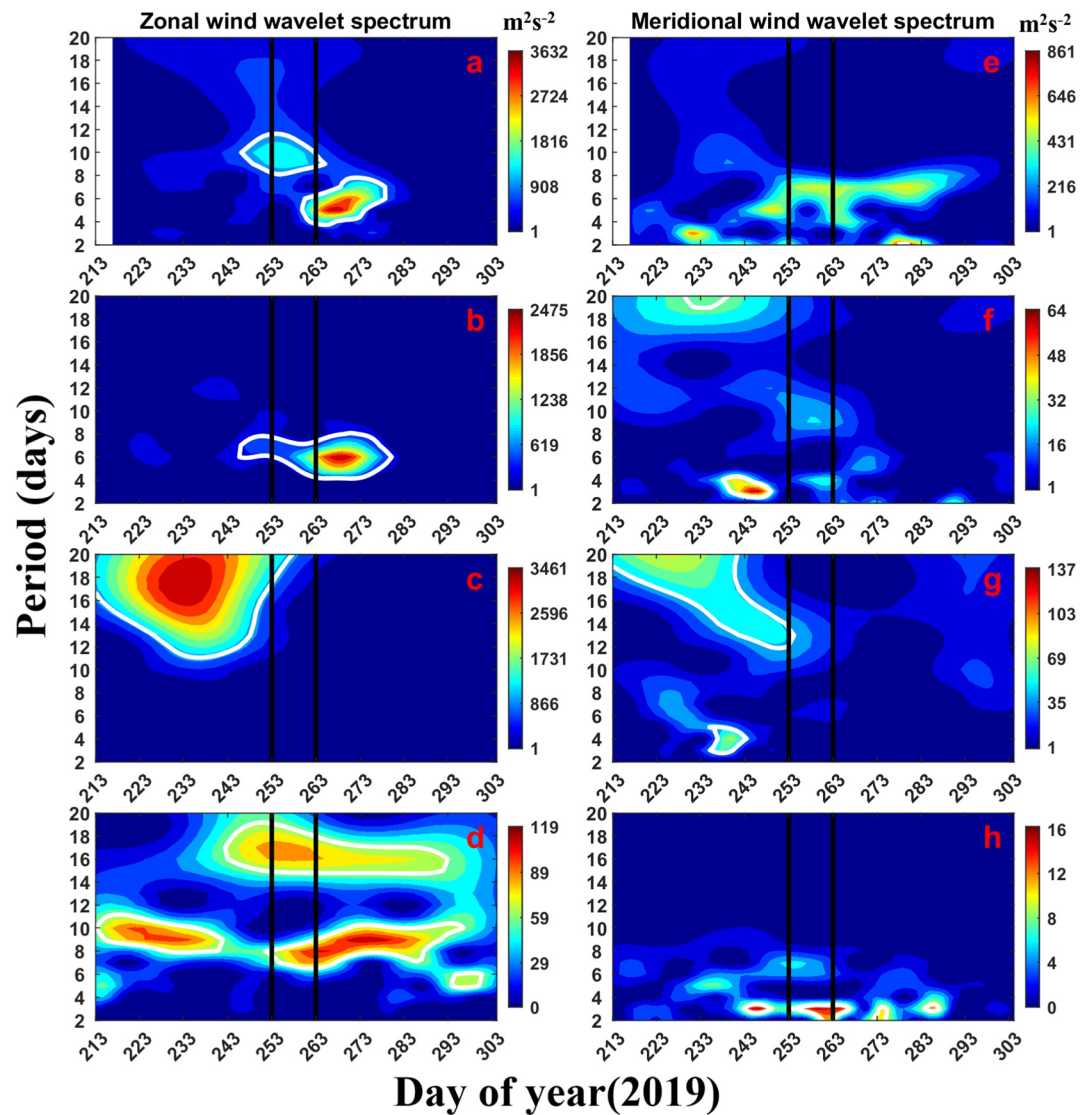


Figure 3. Similar to Figure 2, but shown for CA.

As the wavelet spectra at both observational locations reveal the most dominant periodicities around 6 and 16 days, we further looked into the vertical structure of the two wave components in both wind components in the MLT region as shown in Figure 4. For this purpose, the representative amplitudes of the waves are calculated by using non-linear cosine fit with periods of 6 and 16 days, respectively (Pancheva et al., 2018). As we are interested in looking into the pattern of spatiotemporal variability of the two wave components, consideration of specific periods in the representative amplitude estimation does not affect the interpretation. Figure 4a shows a prominent signature of the Q6DW in the zonal wind during the warming days at CP. The Q16DW in the zonal wind at CP is most active during the pre-warming interval in the MLT region (Figure 4b) although another enhancement is found near top of the MLT during post warming. At CA strong feature of the high Q6DW activity during the late warming phase spread throughout the MLT range can be observed in the zonal wind (Figure 4c). Prominent activity of the Q16DW mostly during the pre-warming interval in the zonal wind at CA is discernible from Figure 4d, although an isolated patch of the wave amplitude can be noted at the lower MLT in the post warming interval. On the other hand, the peak representative amplitude of the Q6DW at CP generally reveals a much weaker signature in the meridional wind as compared to the zonal counterpart as visible at various times in the observational span (Figure 4e). The activity of the Q16DW at CP is found to be notable during pre-warming interval mostly at higher MLT altitudes in the meridional wind as evident in Figure 4f and weaker signature of the

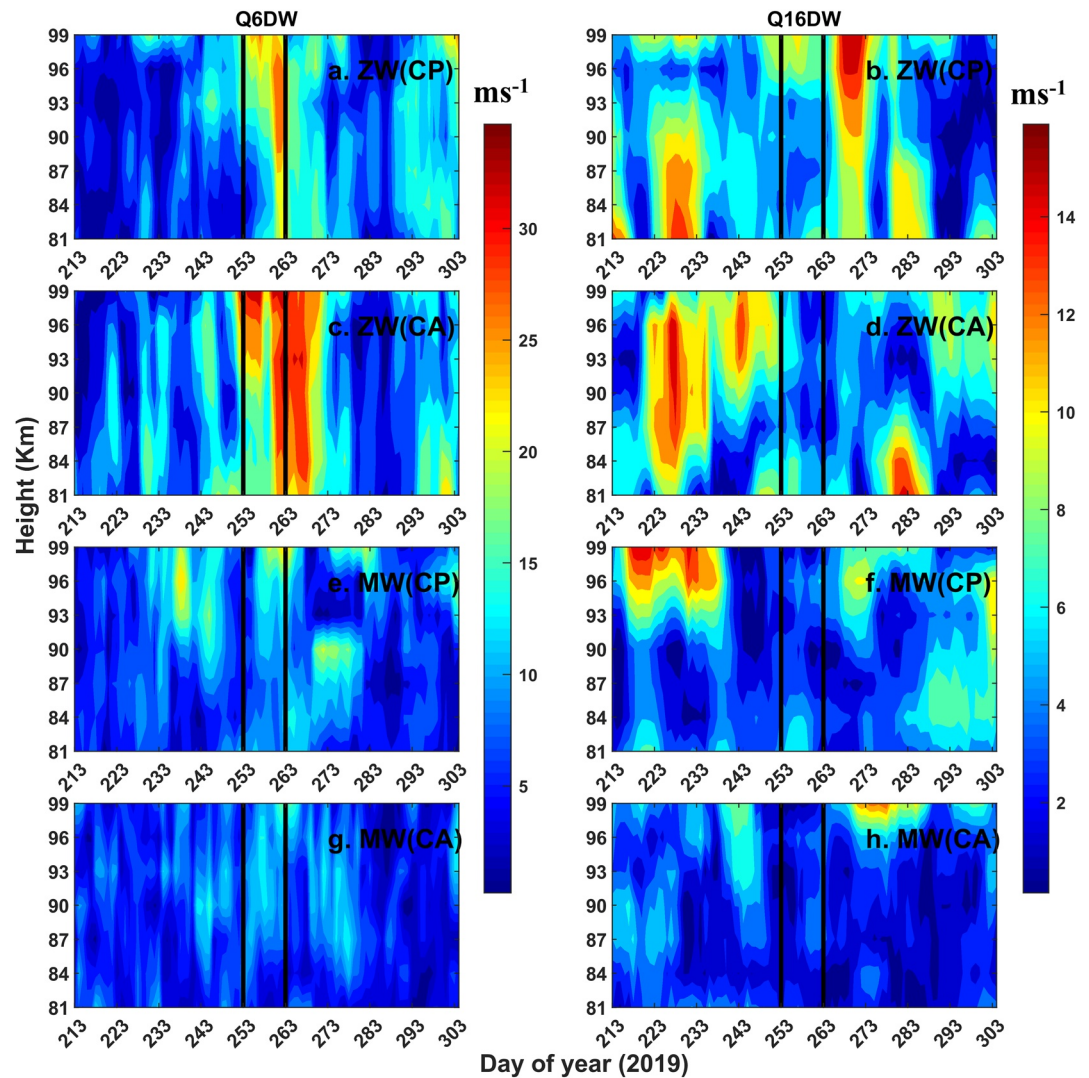


Figure 4. The meteor radar derived representative amplitude of the (a) Q6DW and (b) Q16DW in the zonal wind (ZW) at CP. The same for the (c) Q6DW and (d) Q16DW in the zonal wind at CA. The same for the (e) Q6DW and (f) Q16DW in the meridional wind (MW) at CP. The same for the (g) Q6DW and (h) Q16DW in the meridional wind at CA. Please note the change of scale in the colorbars while comparing.

same is also visible in post warming period. The meridional wind at CA exhibits traces of weak 6-day periodicity around the warming days (Figure 4g). The weak feature of the Q16DW in the meridional wind at CA is mainly observed during pre-warming interval and at higher MLT in post warming span, as seen in Figure 4h. Overall, the representative amplitude of the Q6DW is found to be greater as compared to that of the Q16DW in the MLT region. In general, the Q16DW is observed to be more prominent in pre-warming interval and the Q6DW dominates during post-warming interval consistent with the previous results (Figures 2 and 3) from various altitudes in the middle atmosphere.

To identify the direction of propagation of the traveling PWs around the warming episode, we have utilized the zonal and meridional wind data at 0.02, 1 and 10 hPa at both CP and CA latitude during September 2019 using ERA5 data set. The amplitude of a wave with zonal wavenumber s and period T can be estimated by the non-linear least-square fitting using the following equation.

$$A \cos \left[2\pi \left(\frac{t}{T} + s \frac{\lambda}{360} \right) - \phi \right] \quad (1)$$

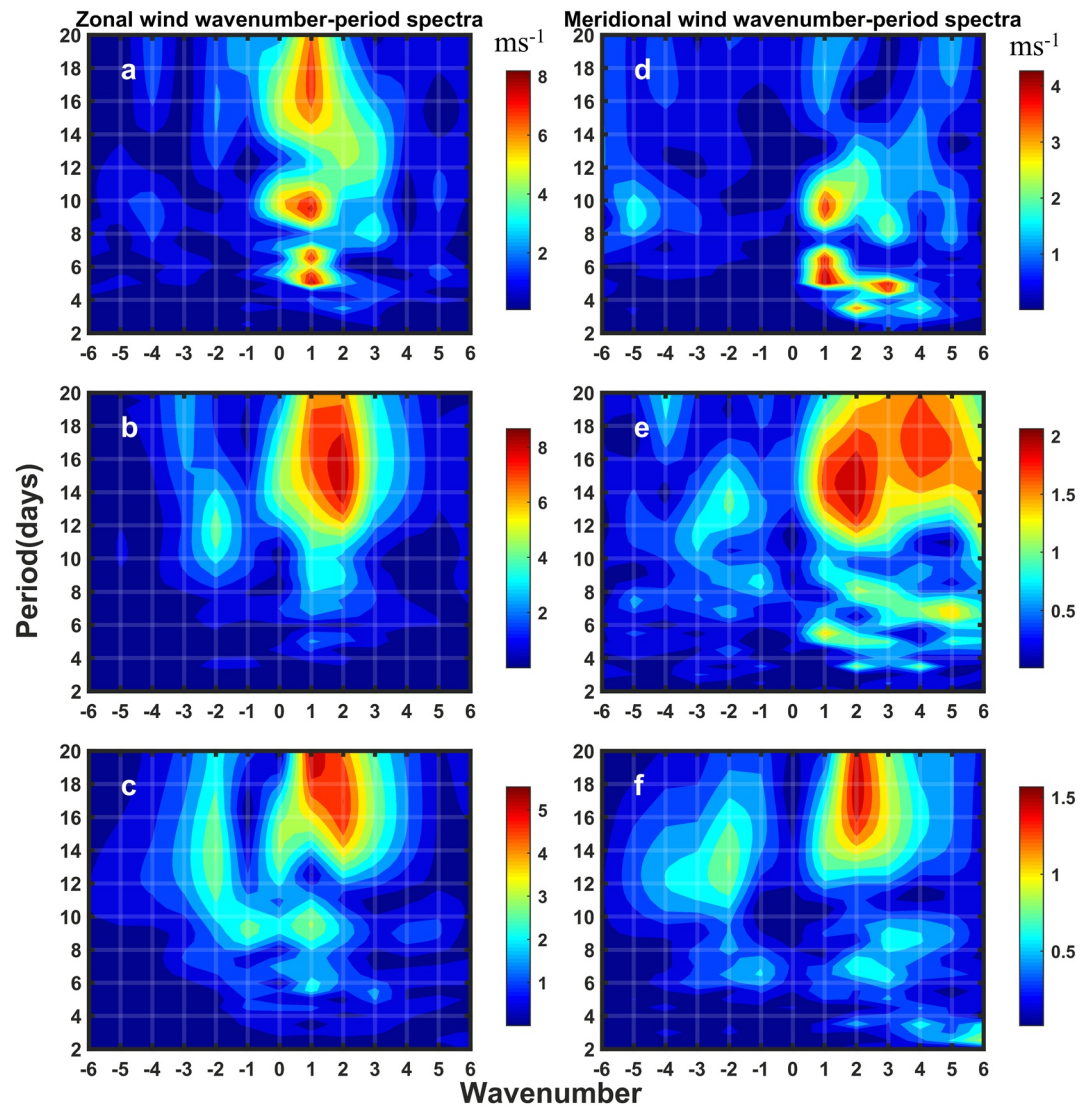


Figure 5. Period versus wavenumber spectra in the zonal wind at (a) 0.02 hPa (b) 1 hPa, (c) 10 hPa and meridional wind at (d) 0.02 hPa (e) 1 hPa, (f) 10 hPa at CP latitude (22.7°S) using ERA5. Please note the change of scale in the colorbars corresponding to each subplot while comparing.

where A is the amplitude of the wave, t is the universal time, λ is the longitude, and ϕ is the phase of the wave. The positive and negative values of s correspond to westward and eastward propagating waves, respectively. The wavenumber-period spectra for the zonal wind over CP at 0.02, 1 and 10 hPa are shown in Figures 5a–5c, respectively. The following features are notable in the wavenumber-period spectra of zonal wind over CP: (a) The zonal wavenumber 1 is the primary westward component of the Q16DW, Q10DW and Q6DW in the mesopause region (0.02 hPa), as observed in Figure 5a. (b) The westward propagating Q16DW with zonal wavenumber 2 is dominant in the zonal wind at 1 hPa pressure level (Figure 5b). (c) In the mid-stratosphere (10 hPa), the Q16DW exhibits a strong westward zonal wavenumber 1 component and a relatively weaker westward zonal wavenumber 2 component as noted from Figure 5c. Similarly, the wavenumber-period spectra of the meridional wind over CP calculated at 0.02, 1 and 10 hPa pressure levels are shown in Figures 5d–5f, respectively. The meridional wind wavenumber-period spectra exhibit following features: (a) The Q10DW mainly consists of westward zonal wavenumber 1, whereas the Q6DW contains both westward zonal wavenumber 1 and 3 in the mesopause (0.02 hPa). Additionally, a weak feature of the Q3DW is found to contain westward zonal wavenumber 2 as seen in Figure 5d. (b) The Q16DW is primarily composed of westward zonal wavenumber 2 in the upper stratosphere (Figure 5e). (c) The Q16DW has a strong westward zonal wavenumber 2 component at 10 hPa (Figure 5f).

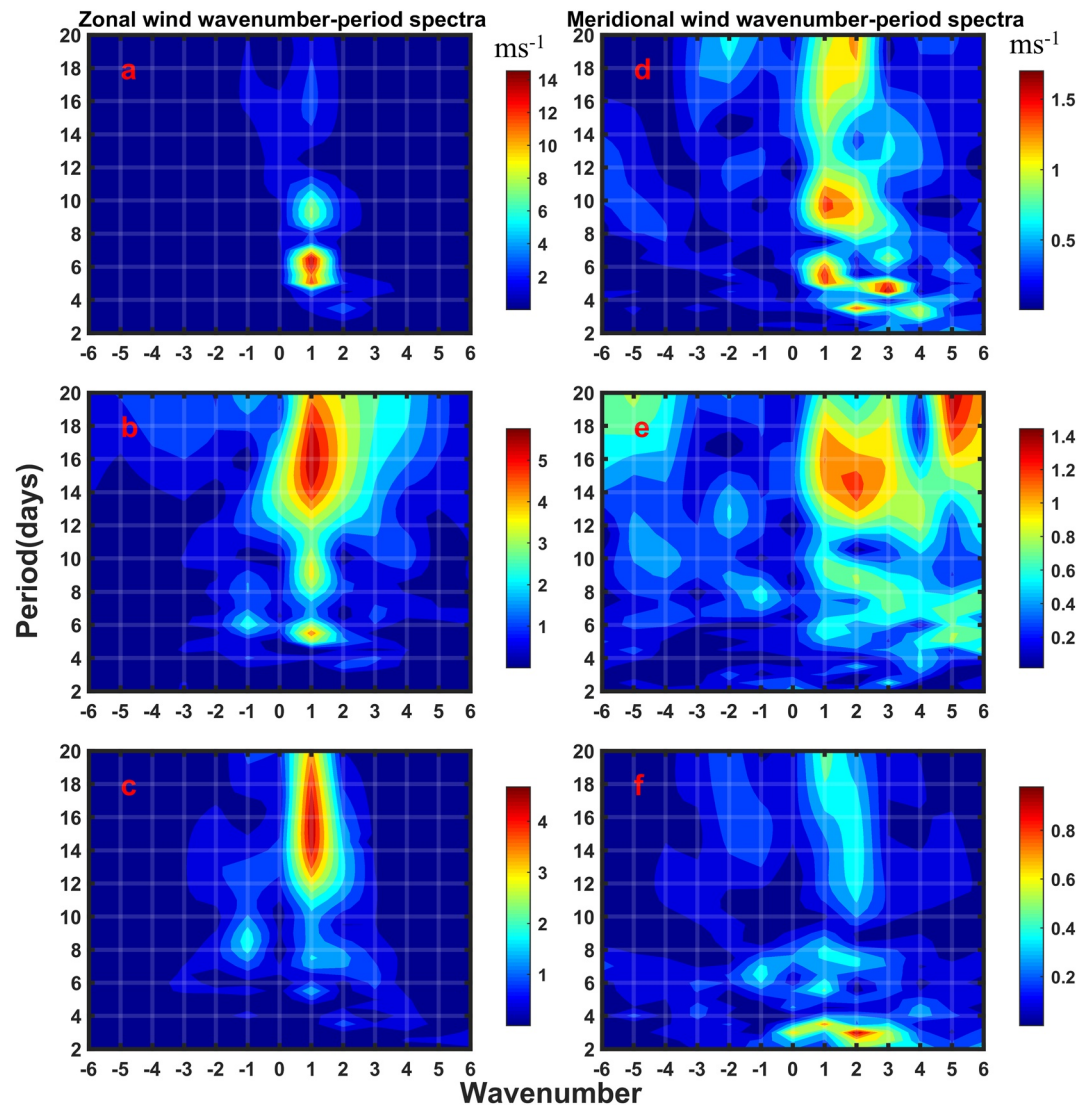


Figure 6. Similar to Figure 5, but at CA latitude (7.4°S).

Similarly, the wavenumber-period spectra of the zonal wind over CA at 0.02, 1 and 10 hPa is illustrated in Figures 6a–6c, respectively. Following features are interesting to note. (a) The Q6DW observed in the zonal wind wavelet spectra at 0.02 hPa travels westward with zonal wavenumber 1, in Figure 6a. A weak signature of the Q10DW with westward zonal wavenumber 1 can be found at 0.02 hPa. (b) The westward propagating zonal wavenumber 1 component is prominent in the Q16DW at 1 hPa (upper stratosphere) as seen in Figure 6b. (c) In the mid-stratosphere (10 hPa), the Q16DW propagates westward with zonal wavenumber 1 (Figure 6c). Figures 6d–6f show the wavenumber-period spectra of meridional wind over CA at 0.02, 1 and 10 hPa respectively. The key features are (a) The primary component of the Q10DW is westward zonal wavenumber 1, and that of the Q6DW is westward zonal wavenumber 1 and 3 in the mesopause (0.02 hPa). Additionally, the Q3DW contains westward zonal wavenumber 2 as seen in Figure 6d. (b) The Q16DW is found to consist of westward zonal wavenumber 2 (Figure 6e). (c) The Q3DW is primarily westward with zonal wavenumber 2 in the mid-stratosphere at 10 hPa (Figure 6f). Overall, the amplitude of the wavenumber-period spectra for the meridional wind is significantly less than that of the zonal wind over both CP and CA. Hence, zonal wind will be considered for further analysis.

The Q6DW and Q16DW is found to be primarily westward with zonal wavenumber 1 component as revealed in the wavenumber-period spectra. Hence, we looked into the temporal variability of the westward zonal wavenumber 1 component of the Q6DW (Q6DW1) and Q16DW (Q16DW1) in the zonal wind during the observational

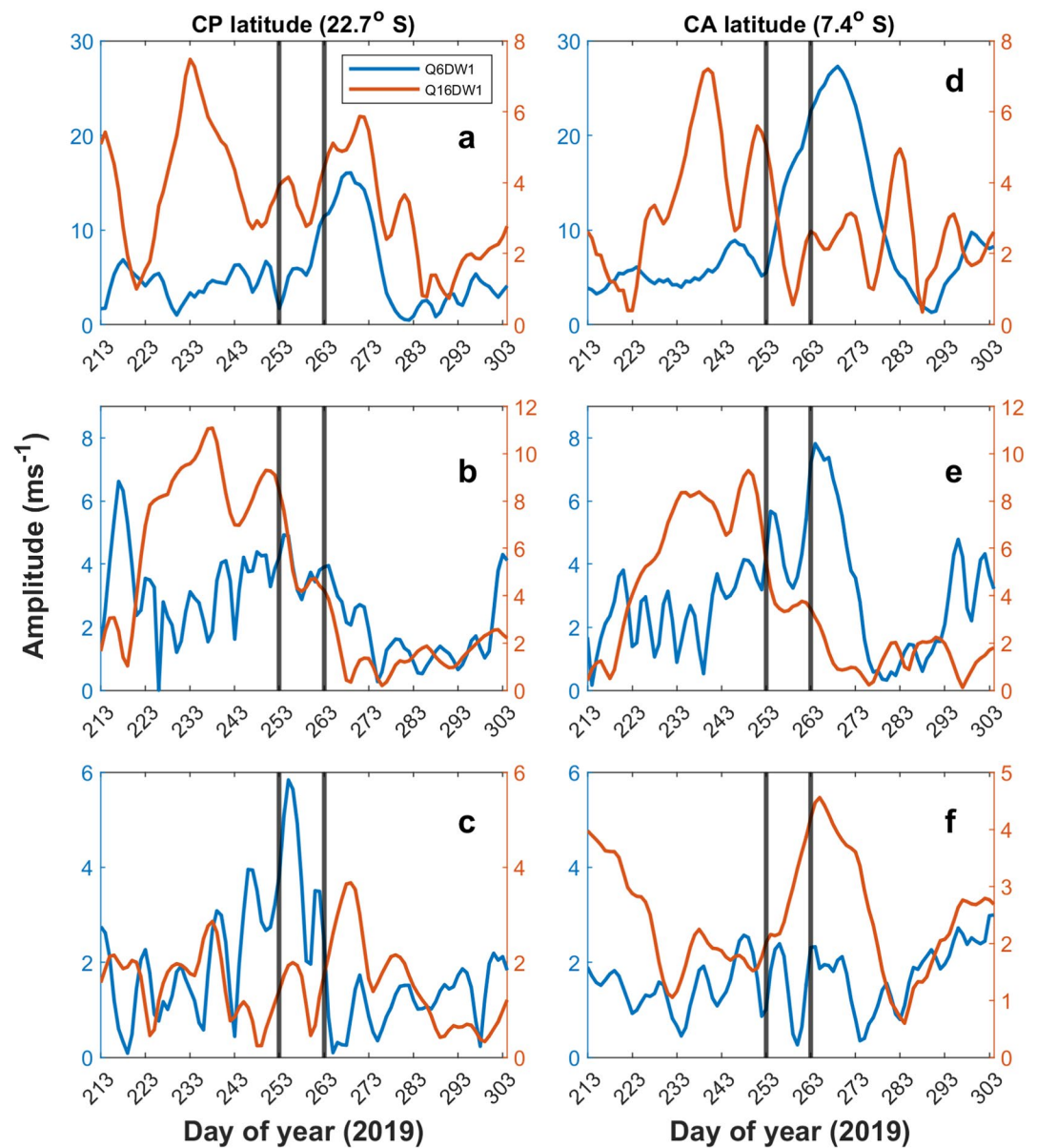


Figure 7. The representative amplitude of the Q6DW1 (blue curve) and Q16DW1 (red curve) in the zonal wind at (a) 0.02 hPa, (b) 1 hPa and (c) 10 hPa at CP latitude (22.7°S). The same at (e) 0.02 hPa, (f) 1 hPa and (h) 10 hPa, but at CA latitude (7.4°S).

interval, as shown in Figure 7. The representative amplitudes of the Q6DW1 and Q16DW1 are derived using Equation 1 considering periods 6 and 16 days and marked by blue and red color, respectively. Figures 7a–7c show the representative amplitude of the Q6DW1 and Q16DW1 at CP latitude at 0.02, 1 and 10 hPa, respectively. Similarly, Figures 7d–7f show the representative amplitude of the Q6DW1 and Q16DW1 in CA latitude at 0.02, 1 and 10 hPa, respectively. At 0.02 hPa, the Q16DW1 shows almost simultaneous enhancement with similar amplitude before warming around DOY 233–243 at both locations. Another peak in postwarming interval is also visible around DOY 273 at CP and DOY 283 at CA with smaller amplitude. The Q6DW1 wave shows simultaneous amplification around DOY-268 at both locations with almost twice amplitude at CA as compared to CP. Overall, the Q6DW1 is found to be significantly higher in amplitude as compared to the Q16DW1.

At 1 hPa broad enhancement peak is found in the Q16DW1 amplitude at both locations during prewarming interval and subsequent weak feature in postwarming interval. The Q6DW1 does not show any consistent enhancement

except a sharp peak on DOY 217 at CP. However, at CA a prominent enhancement is found in the Q6DW1 on DOY 263. It can be noted that the Q6DW1 activity reduces significantly, whereas the Q16DW1 enhances at 1 hPa as compared to that at higher altitude (0.02 hPa).

At 10 hPa the Q16DW1 does not show any notable behavior in response to the warming at CP although it shows warming time enhancement at CA. On the other hand, the Q6DW1 shows amplification during warming at CP and no evident increase at CA unlike the Q16DW1. It can be mentioned that both the wave components are found to be much weaker at 10 hPa as compared to the higher altitudes. Therefore, the Q16DW1 is found to be mainly dominant during prewarming interval and the Q6DW1 enhances during postwarming interval at both tropical and extratropical upper stratosphere and MLT, which is consistent with the wavelet spectra (Figures 2 and 3).

In addition to traveling PWs, characteristics of the stationary planetary waves (SPW) dynamics during the observational span is also investigated. To assess the variability of the dominant wave components in the middle atmosphere, the amplitudes of the SPW corresponding to zonal wavenumbers 1 and 2 in the zonal wind are estimated following the method same as Pancheva, Mukhtarov, Mitchell, Merzlyakov, et al. (2008) and shown in Figure 8. The temporal variation of stationary planetary wavenumber 1 (SPW1) in the SH at 0.02, 1 and 10 hPa is illustrated in Figures 8a–8c. There is evident amplification of the SPW1 at mid latitudes (30–60°S) during the warming and post warming phase near mesopause (0.02 hPa), as seen in Figure 8a. In the upper stratosphere at 1 hPa pressure level (Figure 8b), the SPW1 enhances before the warming at high latitudes. It decays abruptly at the onset of the warming event and remains weaker for the rest of the observational period. At mid latitude, the SPW1 is observed to be active until the warming onset and drastically weakens hereafter. At 10 hPa, the SPW1 exhibits high amplitude at polar latitudes during the warming days and becomes sufficiently weaker after the warming. At mid latitudes, the SPW1 weakens as the warming begins, as seen in Figure 8c. The stationary planetary wavenumber 2 (SPW2) obtained from the daily zonal wind data at 0.02, 1 and 10 hPa are plotted in Figures 8d–8f, respectively. At 0.02 hPa, there is no notable feature in the activity of SPW2 in response to SSW event (Figure 8d). The SPW2 is observed to be active until the end of the warming at 1 hPa in mid latitudes as evident from Figure 8e. The amplitude of the SPW2 is higher at mid latitudes than high latitudes at 1 hPa. The SPW2 remains active before and during warming days but weakens in post warming time at 10 hPa pressure level (Figure 8f). Overall, both components exhibit evident variability in connection with the warming episode with stronger SPW1 as compared to the SPW2, as illustrated in Figure 8.

Breaking of PW causes mixing of air masses between the low and high latitudes (Abatzoglou & Magnusdotir, 2006). As per the availability of the Ertel's potential vorticity (PV) in ERA5 database we show the results of PV up to 1 hPa from the ground. Figures 9a and 9b show the temporal variation of PV averaged over 35–45°W longitudes (considering CP and CA) at 1 hPa and 10 hPa respectively. Such PV maps can give important insights into the temporal dynamics of the meridional air mass mixing. Figure 9a shows a well-stratified layer of increasing absolute PV (APV) value with latitude preceding the warming event at 1 hPa. There is a noticeable intrusion of low APV value across high latitudes during warming days and continues for the remaining period of observation. Few patches of high APV value spread to low latitudes, possibly due to large scale mixing during the warming event (DOY 253–263). Stratified layers of increasing APV value with latitude also exists at 10 hPa (Figure 9b). At this level, notable variability of the APV is observed at high latitude (>70°S) during warming, although at low latitude such effect is not evident.

We further investigate the existence of the baroclinic/barotropic instability during the observational period, as shown in Figures 9c and 9d. According to Charney-Stern-Pedlosky criteria (Pedlosky, 1964), a reversal in the sign of the meridional gradient of PV of the background flow is a necessary but not sufficient condition for the growth of waves. Therefore, an extremum in the latitudinal variability of the PV may indicate barotropic/baroclinic instability. Hence, the meridional gradient of PV averaged over 35–45°W longitudes (covering both locations, CP and CA) at 1 hPa and 10 hPa is calculated. Figures 9c and 9d show only the negative PV gradient at 1 hPa and 10 hPa, respectively to identify the regions of instability. There are several patches of negative PV gradient across all latitudes throughout the observational period at 1 hPa. A dense patch of the same is prominent within the latitudinal domain of 20–40°S during DOY 233 and DOY 263 in Figure 9c may indicate considerable instability. Almost similar features are also observed in the mid-stratosphere at 10 hPa (Figure 9d).

For further investigation the possible source, dissipation and propagation of the dominant wave components, that is, Q6DW or Q16DW are represented by the Eliassen-Palm flux or EP flux (F) and divergence of the EP flux,

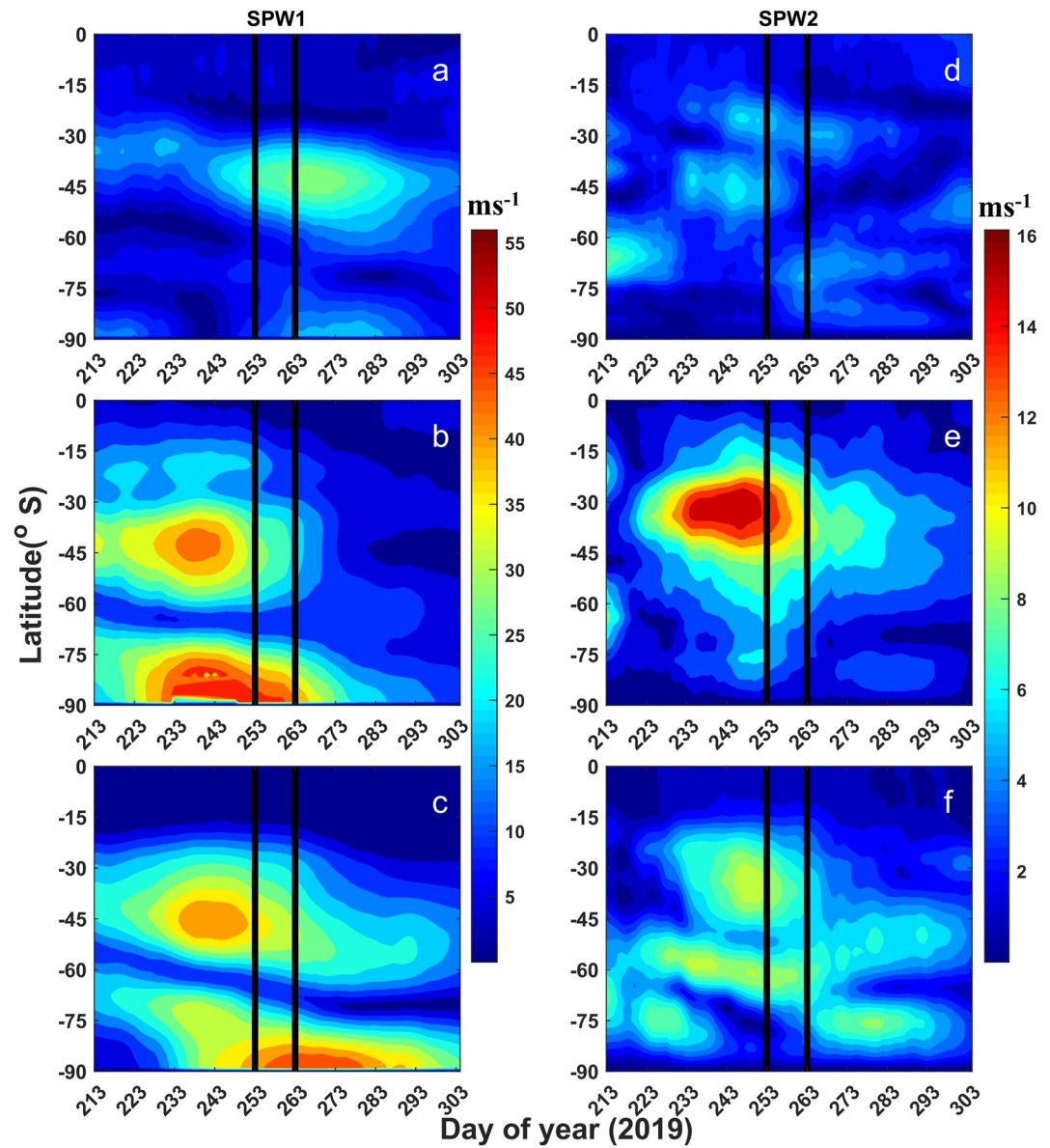


Figure 8. Latitudinal-temporal variation of SPW1 at (a) 0.02 hPa (b) 1 hPa, (c) 10 hPa and SPW2 at (d) 0.02 hPa (e) 1 hPa, (f) 10 hPa estimated from the zonal wind using ERA5 data set. Please note the change of scale in the colorbars while comparing.

$\nabla \cdot \mathbf{F}$ (Andrews et al., 1987; Sivakumar et al., 2004), which are expressed in spherical geometry under quasi-geostrophic approximation as:

$$F = \{f_{(\theta)}, F(z)\} = \left\{ -\rho_o a \cos \phi \left(\overline{v'u'} \right), f \rho_o a \cos \phi \left(\frac{v'\theta'}{\theta_z} \right) \right\} \quad (2)$$

$$\nabla \cdot \mathbf{F} = \frac{1}{a \cos \phi} \left(F_{(\phi)} \cos \phi \right)_{\phi} + (F(z))_z \quad (3)$$

In Equations 2 and 3, overbar denotes zonal mean and prime indicates perturbation due to the Q6DW or Q16DW with all other symbols being as in Andrews et al. (1987). The perturbations due to the Q6DW and Q16DW are calculated by using a band pass filter with passbands of 5–7 days and 14–20 days, respectively in the zonal wind

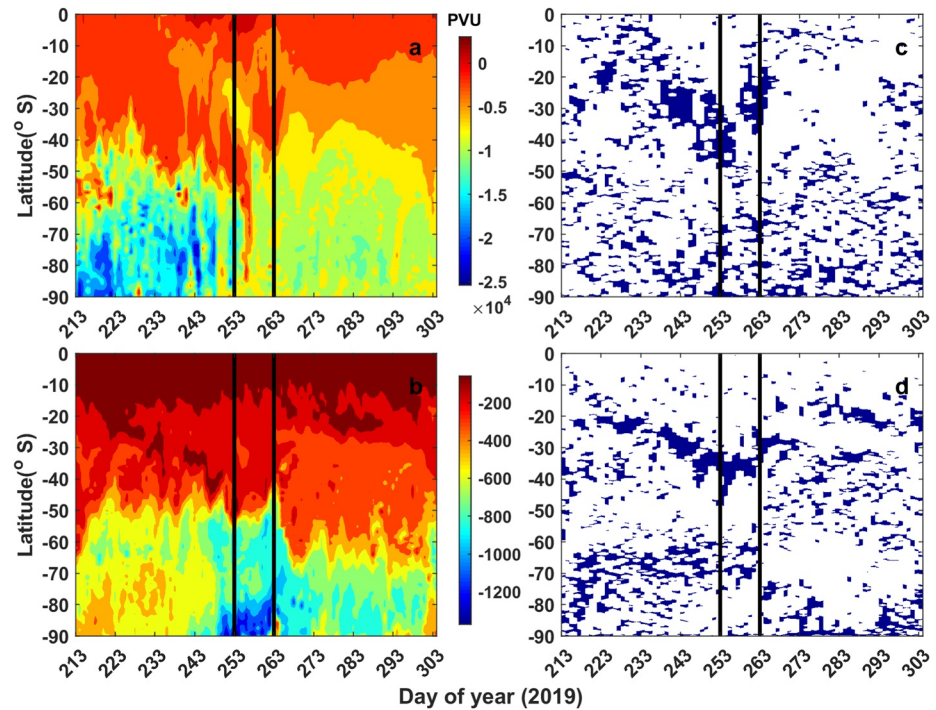


Figure 9. Temporal evolution of PV averaged within 35–45°W with latitudes using ERA5 at (a) 1 hPa and (b) 10 hPa in Potential vorticity unit PVU ($1 \text{ PVU} = 10^{-6} \text{ K m}^2 \text{ kg}^{-1} \text{ s}^{-1}$). The blue contour represents negative value of meridional gradient of PV averaged within 35–45°W at (c) 1 hPa and (d) 10 hPa in PVU per degree latitude. Please note the change of scale in the colorbars while comparing.

(u), meridional wind (v) and potential temperature (θ). Wave driving D is proportional to divergence of EP flux ($\nabla \cdot \mathbf{F}$) as explained in Sivakumar et al., 2004.

$$D = \frac{1}{\rho_0 a \cos \phi} \nabla \cdot \mathbf{F} \quad (4)$$

\mathbf{F} points in the direction of PW propagation (Kanzawa, 1984). Negative D value signifies strong EP flux convergence. The convergence of EP flux vectors indicates the possibility of PW breaking and dissipation of wave energy to the mean flow. Positive D value indicates the source region. We have selected individual days as cases like pre-warming (1 and 6 September), warming (11 and 18 September) and post warming (24 and 30 September) to illustrate the dynamical evolution of wave propagation and zonal wave forcing. Figures 10a–10f shows latitude-height cross-sections of \mathbf{F} (arrow) (both components are scaled appropriately for visibility) and wave driving, D (in contours) corresponding to the Q6DW for prior, during and post warming periods. During the prewarming and warming interval (1–18 September), strong wave convergence is found at polar latitude within 30–60 km and weak wave divergence can be noted at higher altitude, that is, 70–80 km. The wave flux (\mathbf{F}) is found to be predominantly equatorward in the stratosphere (20–40 km) at mid latitudes (30–50°S) during prewarming span (1–11 September). It is noteworthy to mention that concurrent divergence and equatorward wave flux starts enhancing from the peak warming time (18 September) at 70–80 km near 30–50°S. Another zone of equatorward wave flux is prominent in the troposphere, mainly during warming and post warming time (18–30 September) which is limited within 20–50°S although it is not found to be supported by the coincident divergence. Additionally, the wave convergence/divergence at low and mid latitudes is relatively less up to 70 km after the warming (24–30 September). Therefore, the notable point here is the significant equatorward propagation of the Q6DW during post warming period in the upper mesosphere favored by a plausible source in the mid latitude.

Similarly, Figures 11a–11f shows latitude-height cross-sections of wave flux (\mathbf{F}) (arrow) and wave driving, D corresponding to the Q16DW for prior, during and post warming periods. The wave activity in terms of convergence/divergence is high near polar region within 20–60 km vertical range. At mid latitude (50–60°S) the convergence zone near 50 km weakens with time and ultimately changes to a divergence zone from where prominent

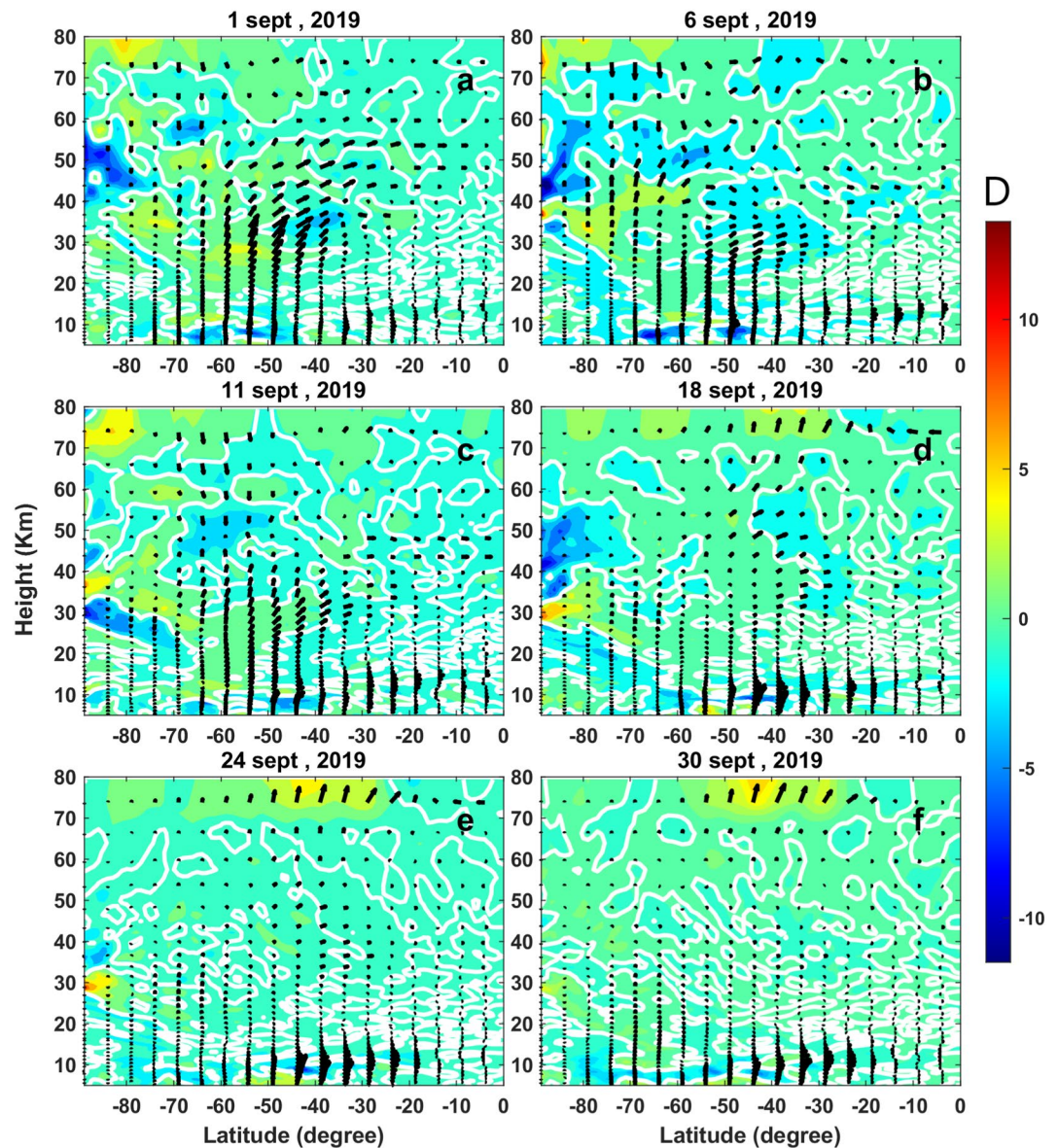


Figure 10. EP flux cross-section of the Q6DW in the meridional plane for prior, during and post warming periods shown for various days. The contour value represents wave driving, D in $\text{m s}^{-1} \text{day}^{-1}$. The white bold curve represents zero value of D .

equatorward wave flux is found to exist until 24 September and hereafter it weakens significantly. Another zone of temporally increasing wave flux is found to maximize near 10–12 km within the latitude range 20–50°S although no supportive concurrent divergence can be identified. Therefore, the most consistent signature in this plot is the gradually increasing Q16DW flux in the stratosphere from mid to low latitudes during the warming period.

4. Discussion

Our present study has illustrated some essential dynamical aspects of a minor SSW event from the SH during September 2019 with meteor radar wind observations from two low latitude Brazilian stations and ERA5 reanalysis data set. The 2019 minor SSW is only the second most robust warming event in the SH reported so far (Noguchi et al., 2020). The current study aims at providing valuable insights into the middle atmospheric dynamics in terms of PWs activity, especially at low latitudes during such a rare event. In the present study, the warming event involves mesospheric cooling at 60°S from DOY 213 until DOY 263 (end of warming). Mesospheric cooling

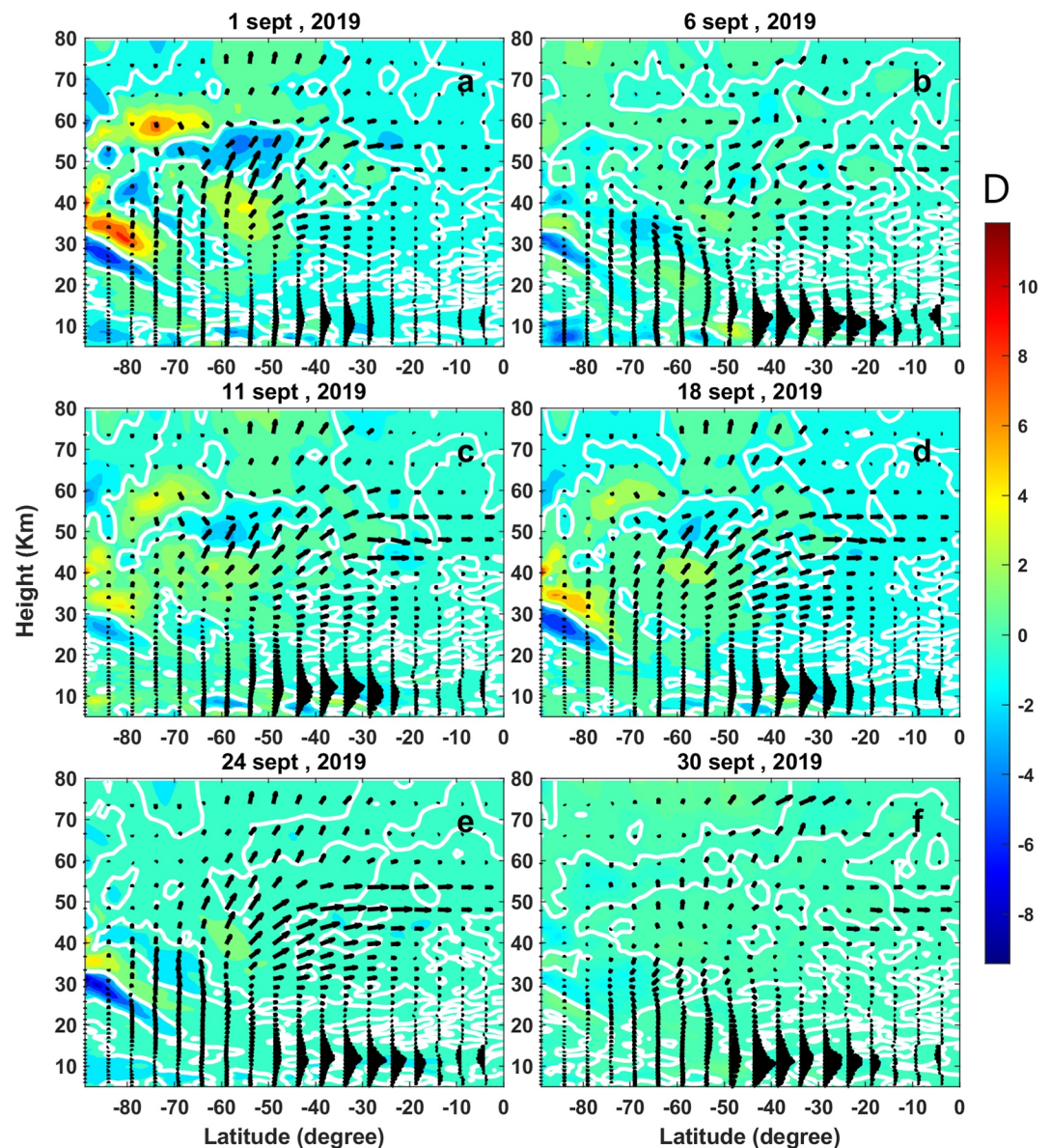


Figure 11. Similar to Figure 10, but for the Q16DW.

during the warming event was reported in the past studies (Duck et al., 1998; Mukhtarov et al., 2007; Schoeberl, 1978). The adiabatic cooling in the polar mesosphere is due to the upward flow of mean residual circulation (Liu & Roble, 2002; Matsuno, 1971). Polar stratospheric warming is concurrent with stratospheric cooling at the present observing tropical latitudes. Tropical stratospheric cooling coincident with stratospheric warming at high latitudes was reported in past studies (Fritz & Soules, 1970; Guharay et al., 2014). Fritz and Soules (1970), with NIMBUS III satellite observations over the NH, inferred that cooling at the tropical latitudes is due to eddy heat transport from high to low latitudes caused by a change in meridional circulation. Noguchi et al., (2020) studied the 2019 SH minor warming event and concluded that the tropical cooling is due to enhanced Brewer-Dobson (BD) circulation. Furthermore, the present minor warming event involves mesospheric warming at low latitudes which is concurrent with mesospheric cooling at high latitudes.

The 2019 SH minor SSW event is characterized by the sudden deceleration of westerly zonal-mean zonal wind from 90 to 10 m s⁻¹ at 60°S, 10 hPa (Lim et al., 2020; Yamazaki et al., 2020). Such a reduction in magnitude from late August to mid-September 2019 is comparable to that of 2002 SH major SSW event accompanying a change

from about 60 to -20 m s^{-1} in late September (Guharay et al., 2014; Lim et al., 2020). In the present event, the reversal of westerly zonal mean zonal wind at high latitude (60°S) initially occurred in the upper mesosphere on 2 September (DOY 245), followed by a descent to the lower altitude reaching 36 km height on 18 September (DOY 261) which is consistent with recent studies by Yamazaki et al. (2020) and Miyoshi and Yamazaki (2020). Since the wind reversal at high latitudes does not occur at 10 hPa, the present event is classified as a minor event in the SH. The zonal mean zonal wind at the present observing latitudes is also affected due to the polar warming in terms of weakening of the eastward wind. Such a feature is prominent around 65 km (mesosphere) over both latitudes of CA and CP. The reduction in the magnitude of westerly zonal wind at around 65 km in low latitudes (Figures 1f and 1h) may be possibly due to the induction of westward momentum to the mean flow by the dissipation of PW at mesospheric altitudes during the warming period.

The observed strong westerly wind before warming as seen in Figures 1d–1h possibly supports and enhances the activity of PW. PW propagates upward provided the background wind speed is below the Rossby critical velocity (Charney & Drazin, 1961). The wavelet spectra at both low latitude locations exhibit almost similar responses in planetary waves pertained to the warming event. The enhanced Q16DW activity at mid and upper stratosphere weakens after the warming days, followed by appearance of the Q6DW in the upper mesosphere (0.02 hPa) and MLT region after the end of warming and remains active for a week (Figures 2 and 3). The Q6DW is generally an equinoctial phenomenon in the MLT region over equatorial and tropical regions when the background wind is moderately westward during April/May and Sept/Oct months (Lima et al., 2005; Kishore et al., 2004). Furthermore, the Q6DW is generally found to be strong in the zonal wind in the MLT region. Additionally, the Q6DW's appearance does not appear to be consistent in the meridional wind with smaller amplitude as compared to the zonal wind counterpart in keeping with previous study (Kishore et al., 2004). The appearance of the Q6DW in the zonal wind after the warming days at the tropical mesosphere may be due to the weakening of westerly zonal mean wind at around 65 km altitude, as seen in Figures 1g and 1h. Although there is a signature of the Q6DW in the meridional wind at CP, it is relatively weak and insignificant at CA. Miyoshi and Yamazaki (2020) studied the behavior of the Q6DW using simulation from Ground-to-topside model of Atmosphere and Ionosphere for Aeronomy (GAIA) during the same warming event and found similar features of the Q6DW supporting the present findings. It is interesting to note that the Q16DW is mainly active in the stratosphere during prewarming conditions, followed by the dominance of the Q6DW in the upper mesosphere during and after the warming. These observations suggest a possibility of dissipation of the Q16DW and subsequent generation of secondary waves in the form of the Q6DW at mesospheric altitudes and MLT region. Occurrence of the secondary PWs in the mesosphere after the 2012 minor SSW event was observed by Chandran et al. (2013). According to the past study, the secondary wave in the MLT after the SSW is due to in situ generation of instabilities in presence of large temperature and wind gradients. In the present study, the reversal of eastward zonal mean zonal wind at 60°S , above 10 hPa (Figure 1f) may be responsible for the enhancement of the Q6DW. In this context, Koushik et al. (2020) suggested that significant wind reversals in the stratosphere following SSWs (2008–2009, 2009–2010 and 2011–2012) in the NH may favor the instability mechanism for the generation of secondary planetary waves. The presence of PW with period 6.5 and 16 days during the same time may suggest some relationship between them (Talaat et al., 2002). The mesospheric warming anomaly during the SSW event at low latitudes as seen in Figures 1c and 1d, is possibly due to the dissipation of the Q16DW, which is mainly active during pre-warming conditions in the stratosphere. Additionally, there exist Q10DW and Q3DW at various times during the observational period. However, they do not seem to offer a striking response to the present minor SSW event. Overall, there is a finite difference in the periodicity of traveling waves observed in the meridional wind than in the zonal wind. This may be because of doppler shift in the frequency of traveling waves due to variation in the background winds (Pancheva, Mukhtarov, Mitchell, Fritts, et al., 2008; Salby, 1981).

The present analysis of propagation direction of the traveling PW (Q16DW, Q10DW and Q3DW) over both CP and CA as seen in Figures 5 and 6 reveals westward PW with zonal wavenumber 1 and 2 as the dominating component. The Q16DW is primarily westward flowing with zonal wavenumber 1 component. Since the Q16DW is mainly active before the initiation of warming event, it may be deemed to play a role in preconditioning the warming event. Additionally, the Q6DW observed primarily at the end of warming is also westward propagating with zonal wavenumber 1. In this context, it should be mentioned that the Q6DW in the atmosphere is basically Rossby wave with zonal wavenumber 1 (Hirota & Hirooka, 1984) which is a robust feature in the middle and upper atmosphere (Hirota & Hirooka, 1984; Lieberman et al., 2003; Pancheva et al., 2018; Talaat et al., 2002). We also observe a strong SPW1 in the stratosphere (10 hPa and 1 hPa) of middle and high latitudes preceding the

warming event that reduces drastically during post-warming conditions, which is in agreement with the previous finding by Yamazaki et al., 2020. Similar features of the SPW2 are observed at 10 hPa (Figure 8f) and 1 hPa (Figure 8e), but with remarkably lower amplitude than that of the SPW1. This indicates salient role of the PWs, predominantly zonal wavenumber 1 (stationary and westward traveling) in preconditioning the SH 2019 minor SSW event.

The barotropic/baroclinic instability is believed to be present at the onset of the warming as evident from the negative meridional gradient at low and mid latitudes (Figures 9c and 9d). The instability diminishes considerably after the warming episode. Such instability helps in the growth of PW activity by extracting energy out of the horizontal/vertical shear of the background flow or equivalently from horizontal temperature gradients (Charney & Stern, 1962). In connection with the generation and maintenance of the 2012/13 SSW, Xu and San Liang (2017) argued that the instability was characterized by the extraction of available potential energy from the vertical or meridional unstable wind structure leading to a reversal of the polar jet. In the present study the existence of instability is also prominent in the zonal mean zonal wind, where the strong westerly jet decelerates at the onset of warming days, as observed in Figures 1d–1h. Furthermore, Tomikawa et al. (2012) indicated the possibility of barotropic/baroclinic growth of PW just after the SSW from the reversed PV gradient in connection with the formation of anomalous westward jet. Theoretical studies of Salby and Callaghan (2001) reported amplification of the 6.5-day wave in an unstable background condition. Lieberman et al. (2003) and Gan et al. (2018) suggested growth of the Q6DW due to baroclinic and barotropic instability during equinoxes. Limpasuvan et al. (2016) reported the generation of westward propagating secondary PWs during SSW through the occurrence of barotropic/baroclinic jet instability. Therefore, consistency of the present findings with the aforesaid previous investigations further corroborates a possible link between the Q6DW and instability of the middle atmosphere. Furthermore, the concurrence of zero wind line at low latitude in Figure 1b and negative PV gradient patch in Figure 8d at 10 hPa during DOY 213–263, suggests a possible link between instability and reversal of zonal mean zonal wind.

The EP flux diagnosis reveals the propagation of the Q6DW and Q16DW from mid and high latitudes to equator in the stratosphere and lower mesosphere. Existence of an intensifying divergence zone with the equatorward Q6DW flux around 70–80 km altitude within the latitudinal range of 30–50°S on the warmest day, that is, 18 September and subsequent interval may indicate a possible source of Q6DW at CP and CA in keeping with the signatures found in Figures 2 and 3 at 0.02 hPa and 90 km altitude. The prominent equatorward Q16DW flux seems to be active until the end of warming days and diminishes during post-warming days. Furthermore, the presence of divergence zone at mid and high latitudes may indicate plausible source region of the Q16DW. Overall, the equatorward Q6DW/Q16DW activity is found to be prominent up to a latitude as low as 20°S (near CP location). Additionally, the impact of the warming is found to be weaker at equatorial latitude (near CA) as compared to the extratropics, which is consistent with the past studies (Hauchecorne & Chanin, 1988; Whiteway & Carswell, 1994).

5. Summary and Conclusions

The present work portrays the PW dynamics in the middle atmosphere during a minor but impactful SSW event in September 2019 observed from two low latitude stations in the Brazilian sector. Although there are studies on convective activity and ionospheric variability during this event, there is hardly any literature related to the impact on the middle atmosphere at low latitudes. Based on the observed features the present warming event can also be termed as high stratospheric warming. The low latitude middle atmosphere shows contrasting character with respect to the high latitude, that is, cooling in the stratosphere coincident with the high latitude warming and warming in the mesosphere concurrent with the high latitude cooling. A strong Q16DW is mostly found to be present before the warming interval and weakens considerably after the warming episode. Another PW component, that is, Q6DW is found in the mesosphere and MLT during the initial days of post warming phase. A handful of traveling PW components, that is, Q16DW, Q10DW, Q6DW and Q3DW are found during the observational period primarily correspond to the westward zonal wavenumber 1 and 2. Furthermore, the current study points out the dominant role of SPWs with zonal wavenumber 1 in preconditioning the 2019 minor SSW event. PV maps in the stratosphere shows significant latitudinal mixing of the air mass. The growth of the Q6DW during the warming is probably associated with baroclinic/barotropic instability. The EP flux reveals propagation of the Q6DW and Q16DW from high and mid to low latitudes associated to the SSW event.

Data Availability Statement

ERA5 data set utilized in the current study is available at <https://www.ecmwf.int/en/forecasts/datasets>. The meteor radar datasets analyzed for the current study are available at <https://figshare.com/s/9eeb223a6429d7e436b4>.

Acknowledgments

The authors acknowledge C. Torrence and G. Compo for the wavelet tool, available at URL: <http://paos.colorado.edu/research/wavelets/>. The present work is supported by the Department of Space (Government of India), National Institute for Space Research, Federal University of Campina Grande, National Council for Scientific and Technological Development (Government of Brazil) and Sao Paulo Research Foundation (Sao Paulo, Brazil). Authors would like to thank Dora Pancheva and three anonymous reviewers for their valuable comments and suggestions.

References

- Abatzoglou, J. T., & Magnusdottir, G. (2006). Planetary wave breaking and non linear reflection: Seasonal cycle and interannual variability. *Journal of Climate*, *19*(23), 6139–6152.
- Andrews, D. G., Holton, J. R., & Leovy, C. B. (1987). *Middle atmosphere dynamics (No. 40)*. Academic Press.
- Chandran, A., Garcia, R. R., Collins, R. L., & Chang, L. C. (2013). Secondary planetary waves in the middle and upper atmosphere following the stratospheric sudden warming event of January 2012. *Geophysical Research Letters*, *40*(9), 1861–1867. <https://doi.org/10.1002/grl.50373>
- Charney, J. G., & Drazin, P. G. (1961). Propagation of planetary-scale disturbances from the lower into the upper atmosphere. *Journal of Geophysical Research*, *66*(1), 83–109. <https://doi.org/10.1029/JZ066i001p00083>
- Charney, J. G., & Stern, M. E. (1962). On the stability of internal baroclinic jets in a rotating atmosphere. *Journal of the Atmospheric Sciences*, *19*(2), 1592–2172. [https://doi.org/10.1175/1520-0469\(1962\)019h0159:OTSOIBi2.0](https://doi.org/10.1175/1520-0469(1962)019h0159:OTSOIBi2.0)
- Dowdy, A. J., Vincent, R. A., Murphy, D. J., Tsutsumi, M., Riggan, D. M., & Jarvis, M. J. (2004). The large-scale dynamics of the mesosphere–Lower thermosphere during the southern hemisphere stratospheric warming of 2002. *Geophysical Research Letters*, *31*(14). <https://doi.org/10.1029/2004GL020282>
- Duck, T. J., Whiteway, J. A., & Carswell, A. I. (1998). Lidar observations of gravity wave activity and arctic stratospheric vortex core warming. *Geophysical Research Letters*, *25*(15), 2813–2816. <https://doi.org/10.1029/98GL02113>
- Fritz, S., & Soules, S. (1970). Large-scale temperature changes in the stratosphere observed from nimbus iii. *Journal of the Atmospheric Sciences*, *27*(7), 10912–11097. [https://doi.org/10.1175/1520-0469\(1970\)027<1091:LSTCIT>2.0.CO](https://doi.org/10.1175/1520-0469(1970)027<1091:LSTCIT>2.0.CO)
- Gan, Q., Oberheide, J., & Pedatella, N. M. (2018). Sources, sinks, and propagation characteristics of the quasi 6-day wave and its impact on the residual mean circulation. *Journal of Geophysical Research: Atmospheres*, *123*(17), 9152–9170. <https://doi.org/10.1029/2018JD028553>
- Goncharenko, L. P., Harvey, V. L., Greer, K. R., Zhang, S.-R., & Coster, A. J. (2020). Longitudinally dependent low-latitude ionospheric disturbances linked to the Antarctic sudden stratospheric warming of September 2019. *Journal of Geophysical Research: Space Physics*, *125*(8), e2020JA028199. <https://doi.org/10.1029/2020JA028199>
- Guharay, A., Batista, P., Clemesha, B., & Sarkhel, S. (2014). Response of the extratropical middle atmosphere to the September 2002 major stratospheric sudden warming. *Advances in Space Research*, *53*(2), 257–265. <https://doi.org/10.1016/j.asr.2013.11.002>
- Guharay, A., & Batista, P. P. (2019). On the variability of tides during a major stratospheric sudden warming in September 2002 at Southern hemispheric extra-tropical latitude. *Advances in Space Research*, *63*(8), 2337–2344. <https://doi.org/10.1016/j.asr.2018.12.037>
- Guharay, A., & Sekar, R. (2012). Signature of latitudinal coupling during a major sudden stratospheric warming in the tropics. *Journal of Atmospheric and Solar-Terrestrial Physics*, *75*, 122–126. <https://doi.org/10.1016/j.jastp.2011.06.010>
- Hauchecorne, A., & Chanin, M. L. (1988). Planetary waves-mean flow interaction in the middle atmosphere: Modelisation and comparison with lidar observations. *Annales Geophysicae*, *6*, 409–416.
- Hersbach, H., Bell, B., Berrisford, P., Hirahara, S., Horányi, A., Muñoz-Sabater, J., et al. (2020). The ERA5 global reanalysis. *Quarterly Journal of the Royal Meteorological Society*, *146*(730), 1999–2049. <https://doi.org/10.1002/qj.3803>
- Hirota, I., & Hirooka, T. (1984). Normal mode Rossby waves observed in the up495 per stratosphere. part i: First symmetric modes of zonal wavenumbers 1 and 2. *Journal of the Atmospheric Sciences*, *41*(8), 12532–21267. [https://doi.org/10.1175/1520-0469\(1984\)041h1253:499NMRWoi2.0.CO](https://doi.org/10.1175/1520-0469(1984)041h1253:499NMRWoi2.0.CO)
- Hocking, W. K., Fuller, B., & Vandeeper, B. (2001). Real-time determination of meteor related parameters utilizing modern digital technology. *Journal of Atmospheric and Solar-Terrestrial Physics*, *63*, 155–169. [https://doi.org/10.1016/S1364-6826\(00\)00138-3](https://doi.org/10.1016/S1364-6826(00)00138-3)
- Hoffmann, P., Singer, W., & Keuter, D. (2002). Variability of the mesospheric wind field at middle and arctic latitudes in winter and its relation to stratospheric circulation disturbances. *Journal of Atmospheric and Solar-Terrestrial Physics*, *64*(8–11), 1229–1240. [https://doi.org/10.1016/S1364-6826\(02\)00071-8](https://doi.org/10.1016/S1364-6826(02)00071-8)
- Kanzawa, H. (1984). Four observed sudden warmings diagnosed by the Eliassen–Palm flux and refractive index. *Dynamics of the Middle Atmosphere*, *307*.
- Kishore, P., Namboothiri, S., Igarashi, K., Gurubaran, S., Sridharan, S., Rajaram, R., & Ratnam, M. V. (2004). Mf radar observations of 6.5-day wave in the equatorial mesosphere and lower thermosphere. *Journal of Atmospheric and Solar-Terrestrial Physics*, *66*(6–9), 507–515. <https://doi.org/10.1016/j.jastp.2004.01.026>
- Kodera, K. (2006). Influence of stratospheric sudden warming on the equatorial troposphere. *Geophysical Research Letters*, *33*(6). <https://doi.org/10.1029/2005GL024510>
- Koushik, N., Kumar, K. K., Ramkumar, G., Subrahmanyam, V., Kishore Kumar, G., Hocking, W. K., et al. (2020). Planetary waves in the mesosphere lower thermosphere during stratospheric sudden warming: Observations using a network of meteor radars from high to equatorial latitudes. *Climate Dynamics*, *54*, 4059–4074. <https://doi.org/10.1007/s00382-020-05214-5>
- Labitzke, K., Naujokat, B., & Kunze, M. (2005). The lower arctic stratosphere in winter since 1952: An update. *Sparc Newsletter*, *24*, 27–28.
- Lieberman, R. S., Riggan, D. M., Franke, S. J., Manson, A. H., Meek, C., Nakamura, T., et al. (2003). The 6.5-day wave in the mesosphere and lower thermosphere: Evidence for baroclinic/barotropic instability. *Journal of Geophysical Research: Atmospheres*, *108*(D20). <https://doi.org/10.1029/2002JD003349>
- Lim, E.-P., Hendon, H. H., Butler, A. H., Garreaud, R. D., Polichtchouk, I., & Shepherd, T. G. (2020). The 2019 antarctic sudden stratospheric warming. *Sparc Newsletter*, *54*, 10–13.
- Lima, L., Batista, P., Clemesha, B., & Takahashi, H. (2005). The 6.5-day oscillations observed in meteor winds over Cachoeira paulista (22.7 s). *Advances in Space Research*, *36*(11), 2212–2217. <https://doi.org/10.1016/j.asr.2005.06.005>
- Limpasuvan, V., Orsolini, Y. J., Chandran, A., Garcia, R. R., & Smith, A. K. (2016). On the composite response of the MLT to major sudden stratospheric warming events with elevated stratopause. *Journal of Geophysical Research: Atmospheres*, *121*(9), 4518–4537. <https://doi.org/10.1002/2015JD024401>
- Liu, H.-L., & Roble, R. G. (2002). A study of a self-generated stratospheric sudden warming and its mesospheric–lower thermospheric impacts using the coupled TIME-GCM/CCM3. *Journal of Geophysical Research: Atmospheres*, *107*(D23). <https://doi.org/10.1029/2001JD001533>

- Matsuno, T. (1971). A dynamical model of the stratospheric sudden warming. *Journal of the Atmospheric Sciences*, 28(8), 14792–21494. [https://doi.org/10.1175/1520-0469\(1971\)028<1479:ADMOTS>2.0](https://doi.org/10.1175/1520-0469(1971)028<1479:ADMOTS>2.0)
- McInturff, R. M. (1978). Stratospheric warmings: Synoptic, dynamic and general circulation aspects. *NASA Reference Publ* NASA-RP-1017:174. Retrieved from <http://ntrs.nasa.gov/archive/nasa/casi.ntrs.nasa.gov/19780010687.pdf>
- Miyoshi, Y., & Yamazaki, Y. (2020). Excitation mechanism of ionospheric 6-day oscillation during the 2019 September sudden stratospheric warming event. *Journal of Geophysical Research: Space Physics*, 125(9), e2020JA028283. <https://doi.org/10.1029/2020JA028283>
- Mukhtarov, P., Pancheva, D., Andonov, B., Mitchell, N. J., Merzlyakov, E., Singer, W., & Murayama, Y. (2007). Large-scale thermodynamics of the stratosphere and mesosphere during the major stratospheric warming in 2003/2004. *Journal of Atmospheric and Solar-Terrestrial Physics*, 69(17–18), 2338–2354. <https://doi.org/10.1016/j.jastp.2007.07.012>
- Noguchi, S., Kuroda, Y., Kodera, K., & Watanabe, S. (2020). Robust enhancement of tropical convective activity by the 2019 Antarctic sudden stratospheric warming. *Geophysical Research Letters*, 47(15), e2020GL088743.
- Pancheva, D., Mukhtarov, P., Mitchell, N. J., Merzlyakov, E., Smith, A. K., Andonov, B., & Murayama, Y. (2008). Planetary waves in coupling the stratosphere and mesosphere during the major stratospheric warming in 2003/2004. *Journal of Geophysical Research: Atmospheres*, 113(D12). <https://doi.org/10.1029/2007JD009011>
- Pancheva, D., Mukhtarov, P., & Siskind, D. E. (2018). The quasi-6-day waves in NOGAPS- ALPHA forecast model and their climatology in MLS/Aura measurements (2005–2014). *Journal of Atmospheric and Solar-Terrestrial Physics*, 181, 19–37. <https://doi.org/10.1016/j.jastp.2018.10.008>
- Pancheva, D. V., Mukhtarov, P. J., Mitchell, N. J., Fritts, D. C., Riggins, D. M., Takahashi, H., & Ramkumar, G. (2008). Planetary wave coupling (5–6-day waves) in the low-latitude atmosphere–ionosphere system. *Journal of Atmospheric and Solar-Terrestrial Physics*, 70(1), 101–122. <https://doi.org/10.1016/j.jastp.2007.10.003>
- Pedatella, N., Chau, J., Schmidt, H., Goncharenko, L., Stolle, C., Hocke, K., et al. (2018). How sudden stratospheric warmings affect the whole atmosphere. *Eos Transactions American Geophysical Union*, 99, 35–38.
- Pedlosky, J. (1964). The stability of currents in the atmosphere and the ocean: Part i. *Journal of the Atmospheric Sciences*, 21(2), 2012–2219. [https://doi.org/10.1175/1520-0469\(1964\)021<0201:TSOCIT>2.0.CO](https://doi.org/10.1175/1520-0469(1964)021<0201:TSOCIT>2.0.CO)
- Rao, J., Garfinkel, C. L., Chen, H., & White, I. P. (2019). The 2019 new year stratospheric sudden warming and its real-time predictions in multiple S2S models. *Journal of Geophysical Research: Atmospheres*, 124(21), 11155–11174. <https://doi.org/10.1029/2019JD030826>
- Salby, M. L. (1981). Rossby normal modes in nonuniform. *Journal of the Atmospheric Sciences*, 38, 18272–21840. [https://doi.org/10.1175/1520-0469\(1981\)038%3c1827:RNMINB%3e2.0.CO](https://doi.org/10.1175/1520-0469(1981)038%3c1827:RNMINB%3e2.0.CO)
- Salby, M. L., & Callaghan, P. F. (2001). Seasonal amplification of the 2- day wave: Relationship between normal mode and instability. *Journal of the Atmospheric Sciences*, 58(14), 18582–21869. [https://doi.org/10.1175/1520-0469\(2001\)058h1858:557SAOTDWi2.0.CO](https://doi.org/10.1175/1520-0469(2001)058h1858:557SAOTDWi2.0.CO)
- Savenkova, E. N., Gavrilov, N. M., & Pogoreltsev, A. I. (2017). On statistical irregularity of stratospheric warming occurrence during northern winters. *Journal of Atmospheric and Solar-Terrestrial Physics*, 163, 14–22. <https://doi.org/10.1016/j.jastp.2017.06.007>
- Scherhag, R. (1952). Die explosionartigen stratosphärenwärmungen des spatwinters 1951-1952. *Ber. Deut. Wetterd.*, 6, 51–63.
- Schoeberl, M. R. (1978). Stratospheric warmings: Observations and theory. *Reviews of Geophysics*, 16(4), 521–538. <https://doi.org/10.1029/RG016i004p00521>
- Sivakumar, V., Morel, B., Bencherif, H., Baray, J.-L., Baldy, S., Hauchecorne, A., & Rao, P. (2004). Rayleigh lidar observation of a warm stratopause over a tropical site, gadanki (13.5 n; 79.2 e). *Atmospheric Chemistry and Physics*, 4(7), 1989–1996. <https://doi.org/10.5194/acp-4-1989-2004>
- Talaat, E. R., Yee, J.-H., & Zhu, X. (2002). The 6.5-day wave in the tropical stratosphere and mesosphere. *Journal of Geophysical Research: Atmospheres*, 107(D12). <https://doi.org/10.1029/2001JD000822>
- Tomikawa, Y., Sato, K., Watanabe, S., Kawatani, Y., Miyazaki, K., & Takahashi, M. (2012). Growth of planetary waves and the formation of an elevated stratopause after a major stratospheric sudden warming in a T213L256 GCM. *Journal of Geophysical Research: Atmospheres*, 117(D16). <https://doi.org/10.1029/2011JD017243>
- Whiteway, J. A., & Carswell, A. I. (1994). Rayleigh lidar observations of thermal structure and gravity wave activity in the high arctic during a stratospheric warming. *Journal of Atmospheric Sciences*, 51(21), 31222–33136. [https://doi.org/10.1175/1520-0469\(1994\)051<3122:R-LOOTS>2.0.CO;2](https://doi.org/10.1175/1520-0469(1994)051<3122:R-LOOTS>2.0.CO;2)
- Xu, F., & San Liang, X. (2017). On the generation and maintenance of the 2012/13 sudden stratospheric warming. *Journal of the Atmospheric Sciences*, 74(10), 3209–3228. <https://doi.org/10.1175/JAS-D-17-0002.1>
- Yamazaki, Y., Matthias, V., Miyoshi, Y., Stolle, C., Siddiqui, T., & Kervalishvili, G. (2020). September 2019 antarctic sudden stratospheric warming: Quasi-6-day wave burst and ionospheric effects. *Geophysical Research Letters*, 47(1), e2019GL086577. <https://doi.org/10.1029/2019GL086577>